J. Coat. Technol. Res., **16** (5) 1263–1281, 2019
https://doi.org/10.1007/s11998-019-00202-9

A novel approach for new cost-saving durable anticorrosive and antibacterial coatings

Walaa M. Abd El-Gawad, Nivin M. Ahmed, Wael S. Mohamed, Eglal R. Souaya

Abstract Multifunctional coatings that perform various actions simultaneously are now of prevailing importance, with zeolites being one of the most useful materials in this field. In this work, Na-P-zeolite was prepared from kaolin and subjected to a cation-exchange process to replace Na^+ by Cu^{2+} and/or Zn^{2+} to achieve anticorrosive and antibacterial effects. In situ emulsion polymerization of vinyl acetate-vinyl versatate (VAc-VEOVA) copolymer at the nanoscale with P-zeolite and Zn-, Cu-, Zn/Cu-cation-exchanged P-zeolites was then applied to obtain P-zeolite-(VAc-VEOVA), Zn-P-zeolite-(VAc-VEOVA), Cu-P-zeolite-(VAc-VEOVA), and Zn/Cu-P-zeolite-(VAc-VEOVA) nanocomposites. Anticorrosive and antibacterial tests were then carried out on films containing the different nanocomposites using laboratory accelerated testing, electrochemical impedance spectroscopy (EIS), and the disc well diffusion method with different types of Gram-positive (G^+) and Gram-negative (G^-) bacteria, revealing that the film containing the mixed (Zn/Cu)-P-zeolite showed the best anticorrosive and antibacterial performance.

Keywords Zeolites, Vinyl acetate, VEOVA 10, Nanocomposites, Copolymerization, Anticorrosive coatings, Antibacterial coatings

W. M. Abd El-Gawad (✉), N. M. Ahmed, W. S. Mohamed
Polymers and Pigments Department, National Research Centre, Dokki, Giza, Egypt
e-mail: chem.walaa@yahoo.com

E. R. Souaya
Chemistry Department, Ain Shams University, Cairo, Egypt

Introduction

Multifunctional coatings can perform different functions simultaneously using one system due to their specific properties. Recently, acrylic waterborne coatings have been most commonly used for such multifunctional applications due to their wide range of mechanical and physical properties.[1–3]

Vinyl ester of versatic acid 10, known as VEOVA 10, is a very attractive monomer for creating such polymers that are required to exhibit a combination of flexibility, hydrophobicity, and very good chemical and ultraviolet (UV) resistance. Therefore, VEOVA 10 is widely used in different applications, including decorative, industrial, and anticorrosive paints, wood coatings, varnishes, and coatings for polyolefins.[4]

VEOVA 10 monomer polymerizes with various other monomers through reaction of its vinyl ester functional group, imparting its specific properties to the copolymers. VEOVA 10 monomer also significantly enhances the performance of vinyl-acetate-based latices by upgrading key properties such as their water and alkali resistance. Manufacture of these VAc-VEOVA copolymers is characterized by easy production with low reactor fouling and high batch reproducibility. Polymers based on the VEOVA 10 monomer exhibit the required balance between hardness and flexibility for the formulation of a wide range of general-purpose and specialty paints with good performance.

The resulting exterior waterborne VAc-VEOVA coatings are widely applied due to their excellent adhesion, durability, and toughness, in addition to their resistance to water, solvents, fire, and alkalis. They also exhibit water repellency, reduced water absorption, high optical transparency, and enhanced mechanical properties and are environmentally friendly, especially considering current restrictions worldwide on solvent-based coatings, which favor those emitting lower amounts of volatile organic compounds (VOC).[4,5]

Zeolites are crystalline aluminosilicates with a three-dimensional porous structure; they have an unusual crystalline structure and a unique ability to exchange their ions with others from outside the structure. A large number of small channels with typical diameter of 0.5 to 0.7 nm are present in the structure, known as microporosity. There are also a number of larger pores, the so-called mesoporosity. The positive ions that are present in the channels can be exchanged for other ions, highlighting the use of zeolites as promising multifunctional materials to host different ions that can offer different functions and their controlled release; For instance, zeolite can act as a host for antibacterial agents such as Cu^{2+}, Zn^{2+}, and Ag^{2+}. Meanwhile, they can also provide good corrosion resistance by increasing the barrier effect of a coating against water vapor by reducing the mobility of the chains and lengthening the pathways for water ingress.[6]

According to Ferrer et al.,[7] the corrosion resistance of AA2023-T3 can be increased by application of a hybrid sol–gel epoxy coating containing NaY zeolite particles double doped with cerium and diethyldithiocarbamate (DEDTC), while Rassouli et al.[8] used Na*X* zeolite as a reservoir for Zn^{2+} and 2-mercaptobenzimidazole to enhance the corrosion protection of an epoxy ester coating. Calabrese et al.[9] compared the corrosion protection performance of different types of zeolite coatings based on a silane matrix on the surface of AA6061 aluminum, reporting high corrosion protection with high hydrophobicity and good adhesion. Bakhsheshi-Rad et al.[10] synthesized a silver-zeolite-doped hydroxyapatite coating (Ag-Zeo-HAp) by using physical vapor deposition (PVD) on a TiO_2-coated Mg alloy and reported that is showed high antibacterial activity towards *Escherichia coli*. Meanwhile, Salim and Malek[11] studied the antibacterial action of regenerated NaY zeolite loaded with silver ions which was thermally treated by cetyltrimethylammonium bromide (CTAB)-modified NaY zeolite and the antibacterial activity of regenerated AgY zeolite in distilled water, both of which showed good antibacterial effect against two bacterial strains that increased with increasing concentration of the Ag cation. Moreover, zeolites are widely used in the coating industry due to their other properties, such as thermal stability, environmental compatibility, resistance to acids and corrosion, porosity, and ready availability.[6]

In situ polymeric nanocomposites consist of an organic polymeric matrix and inorganic filler, one of which is on the nanoscale. Such nanocomposites can exhibit significantly improved mechanical and barrier properties and accordingly offer high performance.[12] Suarez-Martinez et al.[13] prepared a polymer–clay coating consisting of a nanocomposite of montmorillonite (MMT) clay and branched polyethylenimine (BPEI) for corrosion protection of AA2024-T3 to replace chromium conversion coatings, achieving promising results. Meanwhile, Olad and Naseri[14] prepared polyaniline–natural clinoptilolite nanocomposite coatings and reported that they showed good anticorrosive performance in acidic environments in comparison with pure polyaniline coating.

Recently, polymer–zeolite nanocomposites have gained in importance due to their unique chemical and physical properties, attributed to their small size and large surface area with nanoscale dimensions. They may also exhibit novel properties, such as antibacterial resistance, corrosion protection, and thermal stability, which now represents a hot topic in different fields. These polymer–zeolite nanocomposites show markedly improved antibacterial and anticorrosive properties in comparison with microscale composites, making them a novel trend in both antibacterial and anticorrosive coatings.[15,16]

In the work presented herein, Na-P zeolite was prepared from kaolin, then subjected to a cation-exchange process using different cations, namely Zn^{2+}, Cu^{2+}, and their mixture, to achieve anticorrosive and antibacterial activity. Then, the P-zeolite and the cation-exchanged P-zeolites were intercalated in a polymeric emulsion lattice to form polymeric nanocomposites. The four prepared nanocomposites were then integrated into paint formulations containing zeolites in their ingredients to examine their anticorrosive and antibacterial performance when either integrated into the formulation or included in an in situ polymeric matrix.

Experimental

Materials

- Egyptian kaolin is from Kalabsha in Aswan; its chemical composition is 45% SiO_2, 35% Al_2O_3, 3.5% TiO_2 and 1.5% Fe_2O_3 besides traces of other oxides.
- Sodium hydroxide is obtained from Laboratory Rasyan lab (India).
- Commercial sodium silicate has the following formula ($Na_2Si_2O_5$) and is obtained from LYQCI Co. LTD (China).
- Zinc nitrate and copper nitrate of purity 99% were obtained from Win Lab, UK, Alpha Lab, respectively.
- Reagent grade vinyl acetate (VAc) and butyl acrylate (BuA) were supplied by Aldrich.
- Vinyl Versatate (VEOVA10-10 > 99%) was supplied by Shell Chemical Company. The inhibitors in both monomers were removed using inhibitor remover which is a disposable column for removing hydroquinone and monomethyl ether, and the treated monomers were stored at (− 2°C) until used.
- Potassium persulfate (KPS, 99%), sodium lauryl sulfate (SLS.98%), sodium metabisulfite 95% were supplied by Aldrich, and 2,2′-azobis(isobutyronitrile) 98% was obtained from Sigma-Aldrich. The water used was deionized water.

All pigments, extenders, and solvents used were of normal chemical grade, obtained from different local and international companies.

Preparation of P-zeolite

Kaolin preheated at 550–900°C was used as the source of silica and alumina, then an additional mineral silicate source was applied to enrich the Si/Al ratio to achieve the targeted P-zeolite structure. Thereafter, hydrothermal crystallization with NaOH at 70–110°C for 8 h was carried out. The composition of the reactants was $2.87Na_2O$, $1Al_2O_3$, $4.79SiO_2$, and $179.8H_2O$.

Preparation of cation-exchanged P-zeolites

First, 5 g of prepared P-zeolite was stirred with 100 mL 0.1 N Zn or Cu soluble salt or their mixture (Zn/Cu) for 30–45 min. Then, the cation-exchanged zeolites were subjected to filtration and washing. These steps were repeated for several times for each cation to insure complete exchange, then the cation-exchanged P-zeolites were dried at 100°C.

Preparation of (VAc-VEOVA) copolymer nanocomposites by in situ emulsion polymerization

Copolymerization of vinyl acetate (VAc) and vinyl versatate (VEOVA 10) at feed monomer composition ratio of 4:1 and monomer concentration of 25% was achieved via an emulsion polymerization technique in semicontinuous mode under nitrogen with mechanical stirring at 300 rpm. A small amount of butyl acrylate was added to the feed co-monomers to facilitate initiation of the polymerization of the vinyl esters. The reaction was carried out in a 250-mL three-necked flask equipped with a reflux condenser, stainless-steel stirrer, and two separate feed streams, the first for addition of the preemulsion (VAc and VEOVA 10 monomers with sodium lauryl sulfate as emulsifier), and the other for the initiator solution. The following ingredients were added into the round flask successively: part of the emulsifier dissolved in water, 10% of the amount of prepared initiator (potassium persulfate) solution, and 2.5% of the amount of the prepared preemulsion and inorganic additive (1% monomer content). The reaction content was kept in a thermostatic water bath at 85°C. After 10 min, the rest of the preemulsion and dissolved initiator was added dropwise during a period of 3 h. Then, 2,2′-azobis(isobutyronitrile) was added to the reactor during 30 min, and the reaction was continued for another 1 h. Finally, the resulting latex with solid content of 24 ± 1% was cooled to room temperature.[17,18] The recipe for the copolymerization reaction is presented in Table 1.

Paint preparation

The unexchanged and cation-exchanged P-zeolites were integrated into four paint formulations based on P-zeolite-(VAc-VEOVA), Zn-P-zeolite-(VAc-VEOVA), Cu-P-zeolite-(VAc-VEOVA), and Zn/Cu-P-zeo-

Table 1: Ingredients for preparation of in situ zeolite-(VAc-VEOVA) copolymer nanocomposites

Ingredient		Amounts (%)			
Water in initial reactor charge		25	25	25	25
Vinyl acetate		2.0	2.0	2.0	2.0
VEOVA 10		0.5	0.5	0.5	0.5
Butyl acrylate		1.0	1.0	1.0	1.0
Inorganic additives	P-zeolite	0.25	0	0	0
	Zn-P-zeolite	0	0.25	0	0
	Cu-P-zeolite	0	0	0.25	0
	(Zn/Cu)-P-zeolite	0	0	0	0.25
Water in preemulsion		25	25	25	25
Sodium lauryl sulfate		2.0	2.0	2.0	2.0
Potassium persulfate		0.5	0.5	0.5	0.5
Sodium metabisulfite		1.0	1.0	1.0	1.0
Azobisisobutyronitrile		0.25	0.25	0.25	0.25

Table 2: Paint formulations of zeolites with the prepared four nanocomposites

Ingredients (wt.)/paint numbers		P-zeolite nanocomposite	Zn-P-zeolite nanocomposite	Cu-P-zeolite nanocomposite	(Zn/Cu)-P-zeolite nanocomposite
In situ zeolite-(VAc-VEOVA) copolymer nanocomposite	P-zeolite	31	–	–	–
	Zn-P-zeolite	–	31	–	–
	Cu-P-zeolite	–	–	31	–
	(Zn/Cu)-P-zeolite	–	–	–	31
Fe_2O_3		17	17	17	17
TiO_2		5	5	5	5
Kaolin		12	12	12	12
P-zeolite		35	–	–	–
Zn-P-zeolite		–	35	–	–
Cu-P-zeolite		–	–	35	–
(Zn/Cu)-P-zeolite		–	–	–	35
Total pigment		69	69	69	69
Total		100	100	100	100
P/B		2.22	2.22	2.22	2.22

lite-(VAc-VEOVA) nanocomposites. Each paint formulation contained either P-zeolite or one of the cation-exchanged P-zeolite plus titanium dioxide and iron oxide, as presented in Table 2. The pigment/binder (P/B) ratio of the mix was 2.22, and the paints were prepared using a ball mill.

Preparation of steel panels for anticorrosion testing

First, steel was cleaned using clean lintless cloth wet with mineral spirits, rubbing the panel surface vigorously until all soluble and loosely adhered contamination had been removed. Then, the steel panels were rinsed with clean solvent and dried at temperature of 52–93°C (125–200°F) before use or storage. To prevent rusting, panels not used immediately after preparation were wrapped in paper impregnated with dicyclohexylammonium nitrite, or an equivalent volatile corrosion inhibitor (VCI), then placed in a plastic bag or envelope. This preparation is according to ASTM D609-00 (procedure D: solvent wiping). The paints were applied using a film applicator with thickness of 120 μm.

Preparation of specimens for antibacterial testing

Circular plastic specimens with diameter of 1 mm were cut, and the prepared paints applied to them using a brush to form a very thin film. Their antibacterial activity was tested using the disc well diffusion method.

Methods of testing and evaluation of paints

Anticorrosion measurements

Immersion in 3.5% salt solution

A scratch with width of 1 mm was made through the coating along the panel to expose the underlying metal to the aggressive environment. After 28 days of exposure, the panels were evaluated for:

- Degree of rusting (ASTM D 610-00)
- Degree of coating adhesion by cross-cut test (ASTM D 3359-97)
- Degree of blistering on painted steel surfaces (ASTM D 714-07)
- Filiform corrosion resistance by photographic inspection (ASTM D 2803-93)

Electrochemical impedance measurements

The corrosion protection performance of the coatings was investigated by EIS (SP-150, Bio-Logic Science Instruments, France) using the steel panels coated with the paint films as the working electrode, Ag/AgCl as the reference electrode with $E = 240$ mV versus reference hydrogen electrode, and platinum sheet as the auxiliary electrode in 3.5% NaCl solution as electrolyte under a 10 mV sinusoidal potential in aerated solution at room temperature.

Antibacterial measurements (disc well diffusion method)

The antibacterial activity of the tested samples was evaluated using a modified Kirby–Bauer disc diffusion method in the Antimicrobial Laboratory, Faculty of Science, Cairo University.

Briefly, 100 μL of each tested bacterium was grown in 10 mL fresh medium until reaching a count of approximately 10^8 cells per mL. Then, 100 μL microbial suspension was spread onto agar plates corresponding to the broth in which they were maintained.

Plates were inoculated with *Bacillus subtilis* or *Staphylococcus aureus* as Gram-positive bacteria or *Escherichia coli* as a Gram-negative bacteria. The bacteria were incubated at 35–37°C for 24–48 h, then the diameter of the inhibition zone was measured in millimeters. For the disk diffusion test, the zone diameter was measured using slipping calipers according to National Committee for Clinical Laboratory Standards (NCCLS, 1993).

Results and discussion

Characterization of P-zeolite and cation-exchanged P-zeolites

Infrared (IR) spectroscopy

Systematic investigation of the P-zeolite framework structure was carried out in the region of 200–1300 cm^{-1} (Fig. 1; Table 3). The spectra were interpreted by assigning the IR bands to definite structural groups in the P-zeolite framework to estimate the basic zeolite structure.

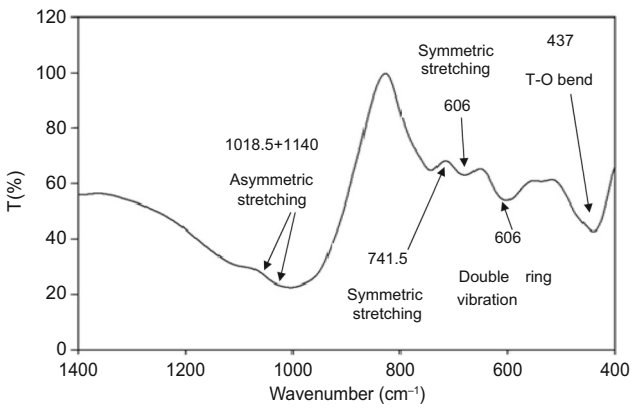

Fig. 1: IR spectrum of P-zeolite

Table 3: IR band assignments

Zeolite	T–O bending at 420–500 cm^{-1}	Double-ring vibration at 500–650 cm^{-1}	Symmetric stretching at 650–820 cm^{-1}	Asymmetric stretching at 950–1250 cm^{-1}
P-zeolite	437	606.5	686 + 741.5	1018.5 + 1140

The IR analysis provides structural information on the zeolite. The mid-infrared region of the spectrum is useful in this regard, since it contains the fundamental vibrations of the framework AlO_4, SiO_4, or TO_4 tetrahedra. Each zeolite appears to exhibit a typical IR pattern. The signals in the spectra can be divided into two classes: (1) those caused by internal vibrations of the TO_4 tetrahedron, which is the major unit and not sensitive to other variations of the structure, and (2) those corresponding to vibrations that may be related to linkages between TO_4 tetrahedra.

The signals observed near 1018.5 and 1140 cm^{-1} are assigned to asymmetric stretching of Si–O or Al–O bonds, while the vibrations at 437 cm^{-1} are related to the deformation mode of the same bonds. The peaks near 686 and 741.5 cm^{-1} are ascribed to symmetric T–O–T vibrations (T = Si, Al) of the P-zeolite framework structure. The peak at 606.5 cm^{-1} corresponds to vibration of the double ring which constitutes the structure of the zeolitic phase; according to Huo, these bands confirm formation of P-zeolite.[19]

X-ray diffraction analysis

Figure 2a shows the X-ray diffraction spectrum for the prepared P-zeolite, clearly showing the main peaks of P-zeolite in good agreement with the data obtained from the standard ASTM card no. 39-219 (Table 4).

Figure 2b–d shows the XRD patterns of the Zn-, Cu-, and Zn/Cu-cation-exchanged P-zeolites, revealing that they all possessed the same structure as the initial P-zeolite without any collapse or destruction, thus the cation exchange process did not affect the degree of crystallinity.

Scanning electron microscopy (SEM)

Figure 3a shows a SEM image of the P-zeolite, revealing pseudospherical morphology as described in literature.[20] In the cation-exchanged P-zeolites (Fig. 3 b–d), Zn^{2+} and/or Cu^{2+} plates with different sizes and shapes appeared around and in between pseudospheres of P-zeolite; e.g., the Zn^{2+} plates were large while the Cu^{2+} plates were agglomerated. This result indicates that the presence of the different cations did not affect the morphology of the P-zeolite but only added new shapes to the zeolite particles.

X-ray fluorescence spectroscopy

X-ray fluorescence (XRF) analysis was applied to determine the oxides present in the prepared zeolites and their concentrations, which can help to determine the cation exchange capacity (CEC) of the cations in the zeolite. The data in Table 5 reveal that the CEC of sodium cation by zinc was about 77.9%, but 92.5% for copper. It is well known from the Periodic Table that the atomic radius of $Na^+ > Zn^{2+} > Cu^{2+}$, which may explain why Na^+ can be more readily exchanged with Cu^{2+} compared with Zn^{2+}.

Characterization of the prepared nanocomposites

Particle size and morphology of the prepared polymers

Figure 4 shows SEM and transmission electron microscopy (TEM) images of the mixed (Zn/Cu)-P-zeolite-(VAc-VEOVA) nanocomposite, revealing particles of two different shapes and sizes due to the presence of Zn^{2+} and Cu^{2+}, in addition to the spherical shape of the copolymer, indicating incorporation of the cation-exchanged P-zeolite particles into the copolymer structure. Additionally, TEM confirmed that the size of the copolymer spheres was on the nanoscale.

Anticorrosion performance of paints containing P-zeolite and cation-exchanged P-zeolites

Immersion testing

After applying the paints onto steel panels, accelerated corrosion testing was conducted for 28 days in 3.5% NaCl. After the end of the exposure period, visual inspection of the films according to ASTM patterns was applied to detect blistering, adhesion, and rust under each film. The results of the immersion test (Table 6; Fig. 5) revealed that the paint films with (VAc-VEOVA) copolymer exhibited improved adhesion due to the good adhesion of VEOVA, in accordance with literature.[4] The appearance of blisters was limited, and the results showed that the corrosion protection behavior of the paint films containing the cation-exchanged P-zeolites were better than that with P-zeolite, with the best result being shown by the film containing the (Zn/Cu) P-zeolite.

EIS results

Electrochemical impedance spectroscopy was used as a quantitative technique to confirm the results obtained by the laboratory immersion test.

Nyquist plots of the impedance spectra were analyzed by fitting the experimental data using a simple Randles circuit model $[R_s + C_{dl}/R_{ct})]$ (Fig. 6). The equivalent circuit represents the corrosion process on the bare surface, consisting of the electrolyte resistance (R_s) in series with the double-layer capacitance (C_{dl}) and charge-transfer resistance (R_{ct}) in parallel with one another.

The evolution of the Nyquist plots for the paint films after 1, 7, 14, 21, and 28 days in 3.5% NaCl and the data for their corrosion protection behavior are shown in Fig. 7 and Table 7, respectively. These results reveal that the charge-transfer resistance (R_{ct}) of the paint film containing the (Zn/Cu)-P-zeolite was high, reaching 38,000 Ω cm^2 at the beginning of immersion,

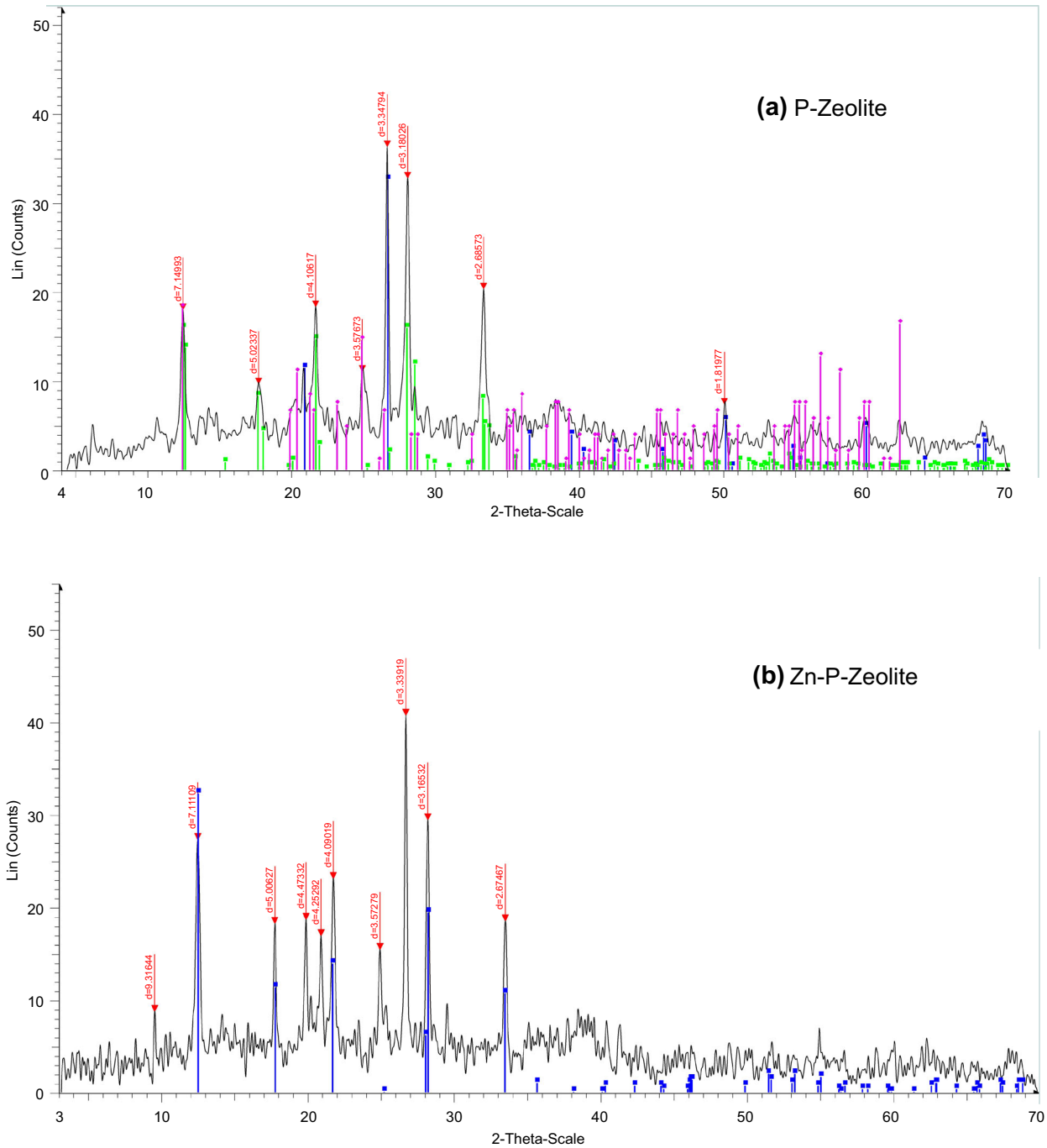

Fig. 2: XRD spectra of (a) P-zeolite and after cation exchange with (b) Zn, (c) Cu, and (d) Zn/Cu

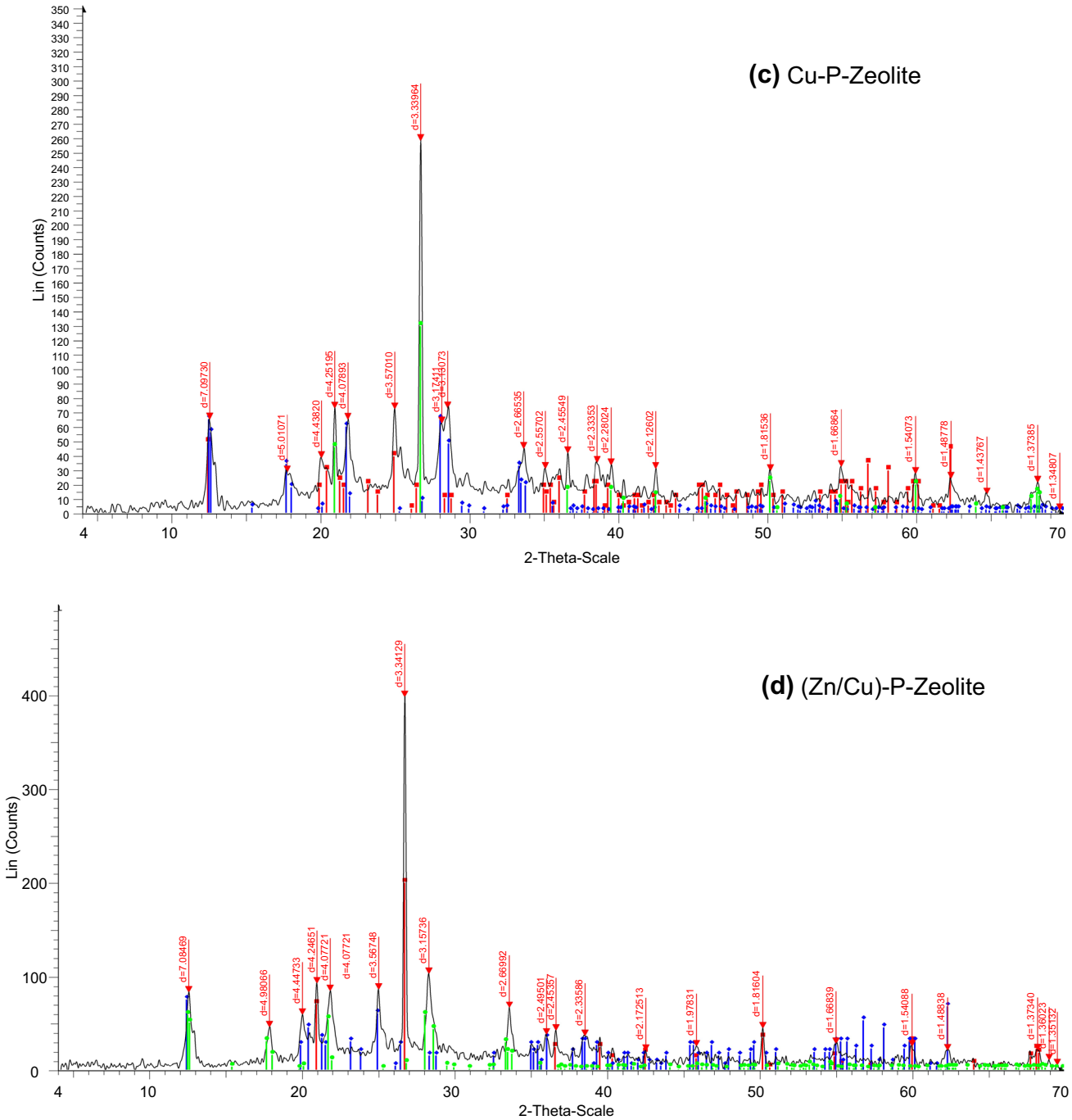

Fig. 2: continued

followed by a gradual decrease during the immersion period until it reached 15,000 Ω cm^2. This variation may reflect the penetration of water through the coated film and the associated mechanisms.

At the beginning of the immersion, water did not reach the metal–coating interface, therefore no corrosion appeared under the coated films and the charge-transfer resistance increased with the immersion time. However, in the interval between 21 and 28 days, corrosive ions and water reached the metal–coating interface and corrosion began underneath. This explanation is in good agreement with the diffusion pro-

Table 4: XRD bands of the prepared P-zeolite

Standard ASTM card no. 39-219		Prepared P-zeolite	
2θ (°)	*d* value (Å)	2θ (°)	*d* value (Å)
12.455	7.1	12.5	7.144
17.649	5.01	18	5.02
21.657	4.10	21.5	4.10
25.056	3.26	26.5	3.34
33.35	2.05	33.5	2.03

cesses of water through coatings, which can be divided into two stages, namely the initial and saturation stages.

In the initial stage, the charge-transfer resistance increased with the immersion time then decreased due to the diffusion of corrosive materials; when the saturation stage was reached, the charge-transfer resistance remained stable.[8,21] Comparing these results with literature,[8] it is clear that the resistance remained high until the end of the immersion period, indicating good corrosion protection behavior. This result is

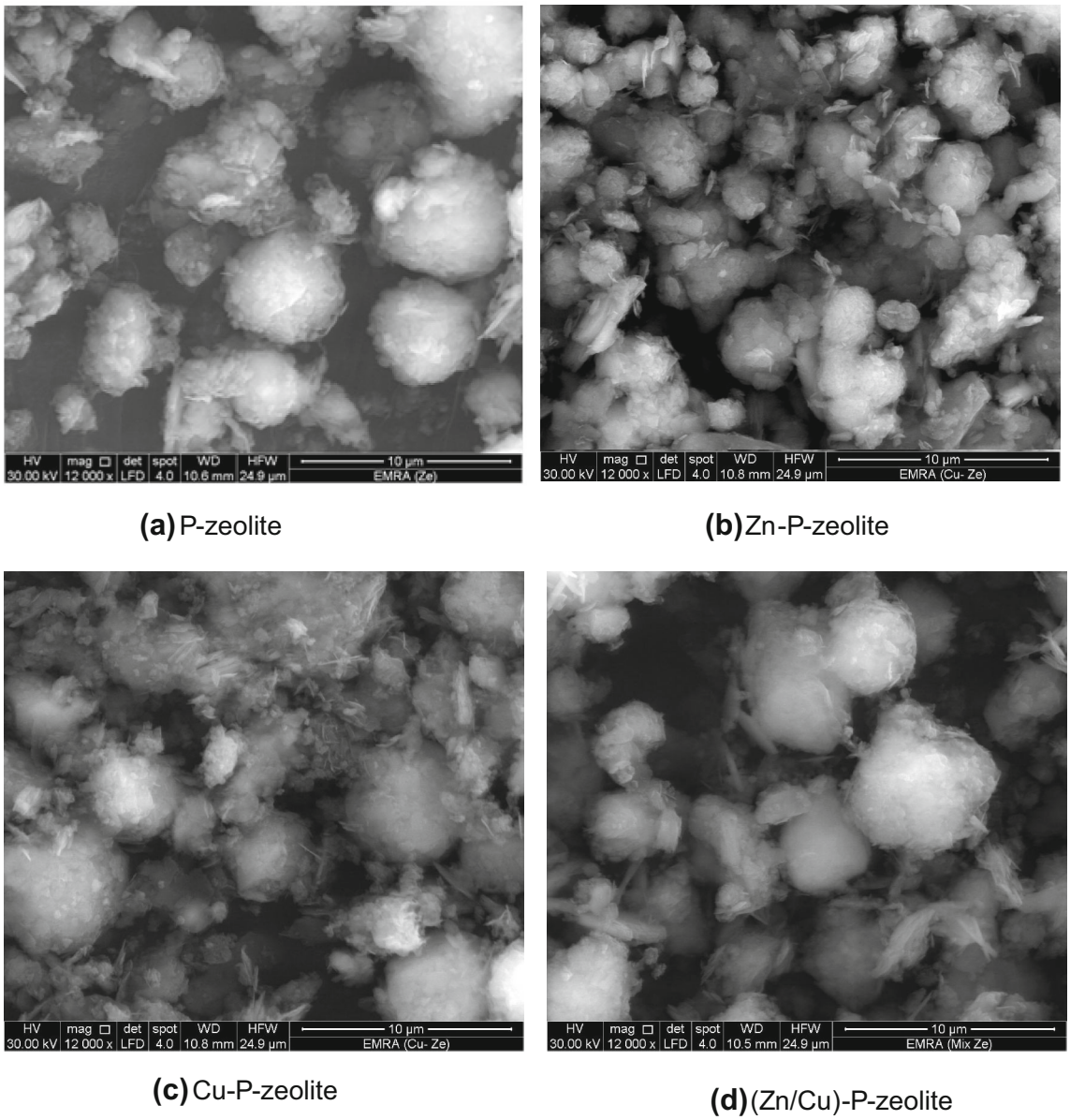

Fig. 3: SEM images of (a) P-zeolite and after cation exchange with (b) Zn, (c) Cu, and (d) Zn/Cu

Table 5: XRF results of P-zeolite and cation-exchanged P-zeolites

Main constituent (wt.%)	P-zeolite	Zn-P-zeolite	Cu-P-zeolite	(Zn/Cu)-P-zeolite
SiO_2	52.11	52.75	49.93	51.77
Al_2O_3	30.55	26.96	29.222	26.69
TiO_2	2.11	1.85	2.10	1.88
Fe_2O_3	2.11	1.90	2.12	1.84
MnO	0.01	0.02	0.01	0.01
CuO	0.008	0.010	9.235	10.605
ZnO	0.018	7.777	0.034	2.698
NiO	0.014	0.014	0.016	0.012
MgO	1.54	1.24	1.44	1.20
CaO	1.03	0.56	0.62	0.49
SrO	0.022	0.020	0.021	0.020
Na_2O	9.98	6.94	4.32	2.29
K_2O	0.08	0.12	0.08	0.11
Ga_2O_3	0.006	0.010	0.004	0.04
Y_2O_3	0.009	0.008	0.009	0.008
Nb_2O_5	0.014	0.013	0.016	0.015
PbO	–	0.019	0.015	0.021
ZrO_2	0.105	0.104	0.118	0.112
CeO_2	0.032	–	0.032	0.026
Co_3O_4	0.006	–	–	–
P_2O_5	0.06	0.06	0.07	0.06
SO_3	0.12	0.02	0.53	0.10
Cl	0.03	0.02	0.03	–

promising because it indicates that, after longer exposure times and as the electrolyte penetrates the coatings more rapidly, notable concentrations of Zn^{2+} and Cu^{2+} can be released from the zeolite cavities, forming a distinct protective layer of $Zn(OH)_2$ and $Cu(OH)_2$. Accordingly, the cavities in the zeolite act as a reservoir for Cu^{2+}, controlling its release and allowing its spontaneous reaction with OH^- groups to form the hydroxide. Also Zn^{2+} ions can reach anodic sites on the metal surface, causing a significant decrease in the oxidation reaction rate of the metal and reducing the number of active sites available for electrochemical reactions. In addition, the different particle sizes of these two cations may play an important role in the superior inhibition performance by forming a more compact film that can increase the barrier effect.[22,23]

Additionally, good corrosion protection performance was exhibited by all the different nanocomposites, due to the carbon-rich structure of the VEOVA 10 monomer that offers high polymeric hydrophobicity. This property can be exploited to produce water-repellent films and enhance the anticorrosion performance, especially when copolymerizing the VEOVA monomer with vinyl acetate to form the (VAc-VEOVA) copolymer.[4]

On the other hand, copolymerization of VEOVA 10 monomer and vinyl acetate leads to polymers with monomer units distributed randomly along the chain. The unique, highly branched, carbon-rich structure of the monomer drastically protects its ester group from being hydrolyzed. The most important effect is that it also protects neighboring acetate groups, improving the hydrolytic stability of the polymer. This protection phenomenon is called the ''umbrella effect'' and enables such copolymers to be successfully used as paint binders for corrosion protection,[4] as seen in Fig. 8.

Antibacterial results for cation-exchanged P-zeolites and their paint formulations

The antibacterial activity of both the cation-exchanged P-zeolites and their paint films are shown in Figs. 9 and 10 and presented in Table 8. This test was performed by subjecting the cation-exchanged P-zeolite or paint

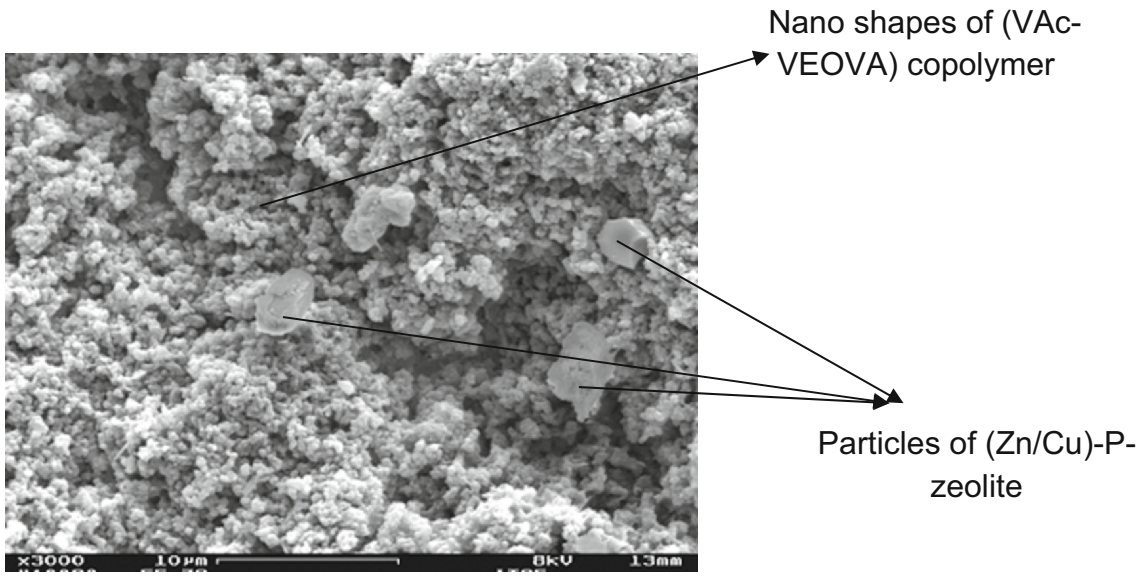

(a) SEM

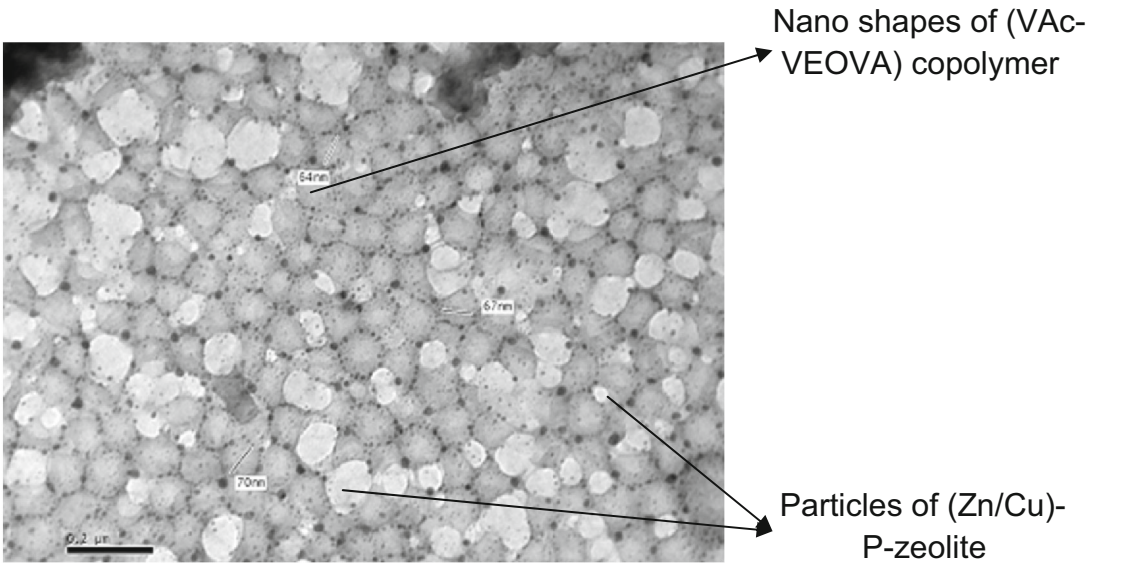

(b) TEM

Fig. 4: (a) SEM and (b) TEM images of (Zn/Cu)-P-zeolite-(VAc-VEOVA) copolymer nanocomposite

Table 6: Corrosion resistance of paint formulations containing zeolites

Test	P-zeolite nanocomposite	Zn-P-zeolite nanocomposite	Cu-P-zeolite nanocomposite	(Zn/Cu)-P-zeolite nanocomposite
Degree of blistering	8F	2F	8F	10
Degree of rusting	2G, 33%	7G, 0.3%	3P, 3%	10
Adhesion	Gt2	Gt0	Gt0	Gt0

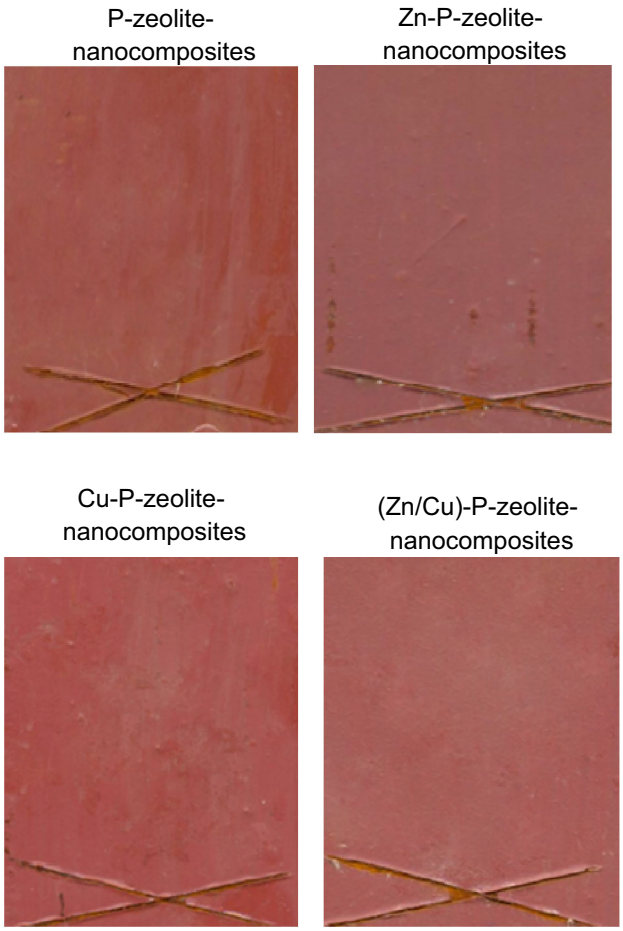

Fig. 5: Results of laboratory corrosion testing of paint films after 28 days of immersion in 3.5% NaCl

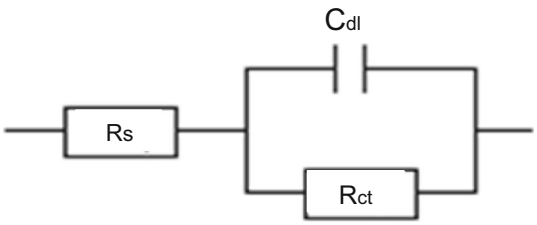

Fig. 6: Equivalent electrical circuit used to fit the EIS data for the coatings

film to two Gram-positive (G^+) and one Gram-negative (G^-) bacterial strain using the disc well diffusion method. In this work, the Gram-positive bacterial strains were *Bacillus subtilis* and *Streptococcus faecalis*, while the Gram-negative strain was *Escherichia coli*.

Antibacterial results for cation-exchanged P-zeolites

According to the results in Fig. 9 and Table 8, the (Zn/Cu)-P-zeolite strongly inhibited the growth of both G^+ and G^- bacterial strains, with inhibition zones for *Bacillus subtilis*, *Streptococcus faecalis*, and *Escherichia coli* of 18, 19, and 21 mm, respectively.

Cu-P-zeolite showed an inhibition zone of 17 mm for the two G^+ bacteria and 19 mm for the G^- bacterium. The inhibition zones of the Zn-P-zeolite were the smallest, with no inhibition zone being detected for the two G^+ bacterial strains and 10 mm for the G^- strain. This proves that Zn^{2+} and/or Cu^{2+} exhibited a synergetic effect in inhibiting the bacterial activity. These results can be explained based on the following mechanisms:

Both Cu^{2+} and Zn^{2+} could resist the bacterial activity by associating themselves tightly with soft bases found in proteins, e.g., sulfhydryl (R–SH) groups, damaging enzyme activity. Accordingly, the cell structure changes, affecting the normal physiological processes and preventing activity of the microorganism.

Additionally, Cu^{2+} produces reactive oxygen species (ROS) and depletes antioxidants, because of the oxidation–reduction process between Cu^+ and Cu^{2+}, causing oxidative stress to the bacterial cells and enhancing the antibacterial activity of the material. This can be explained by production of hydroxyl radicals ($OH^{\bullet}$) that break proteins by carbonylation, and peroxidate lipids and nucleic acids, thereby deforming and destroying DNA.[24–27] These mechanisms are presented schematically in Fig. 11.

From the results described above, it can be deduced that the antibacterial activity of Cu^{2+} is greater than that of Zn^{2+}, because it can inhibit bacterial activity through mechanisms associated with both soft bases of proteins and oxidation–reduction between Cu^+ and Cu^{2+}.

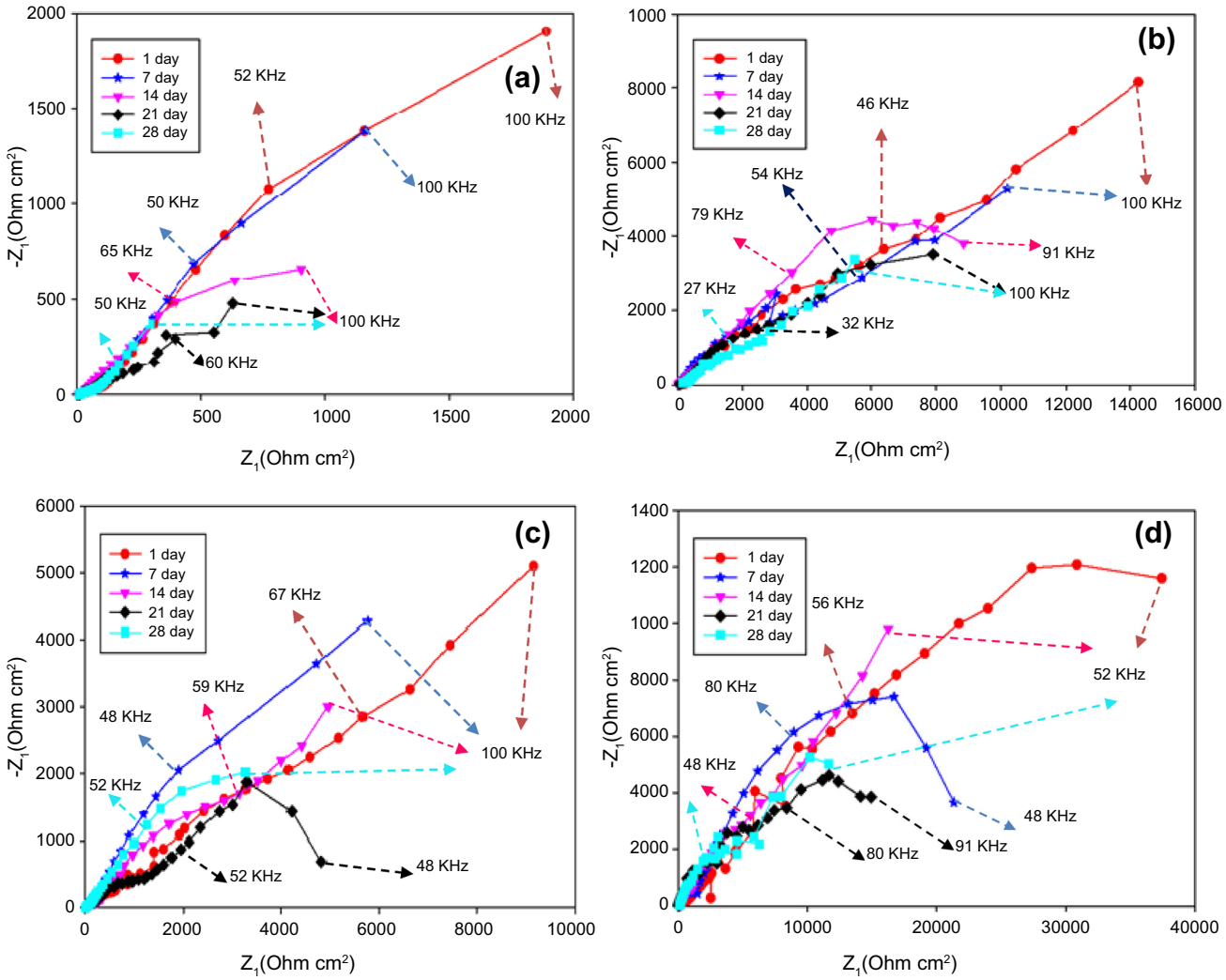

Fig. 7: Nyquist plots of paint formulations containing (a) P-zeolite nanocomposite, (b) Zn-P-zeolite nanocomposite, (c) Cu-P-zeolite nanocomposite, and (d) (Zn/Cu)-P-zeolite nanocomposite during immersion in 3.5% NaCl for 28 days

Antibacterial results for paint formulations

The antibacterial effect of the paint films based on the four nanocomposites is shown in Fig. 10 and Table 8. The inhibition zones of the painted specimens containing the Zn, Cu, and (Zn/Cu)-P-zeolite-(VEOVA-VAc) nanocomposites showed results of 13R–16 mm, 25–30 mm, and 26–32 mm, respectively.

It is clear that integration of the cation-exchanged P-zeolites into the nanoemulsions increased their antibacterial performance in comparison with the cation-exchanged P-zeolite powder itself, which can be attributed to the effect of the nanoemulsions.

Adsorption of bacteria onto the surface of the polymer causes diffusion of water through the polymer matrix, leading to release of Zn^{2+} and/or Cu^{2+} cations to the surface. This leads to (twofold) higher antibacterial action due to the presence of zeolite in both the polymer itself and as an ingredient in the paint, resulting in severe destruction of the bacterial membrane.[24] Also, nanoemulsions are considered to represent a versatile solution for both precise and timed

Table 7: EIS data for paint formulations containing zeolites

Sample	Immersion duration	R_s (Ω cm^2)	R_{ct} (Ω cm^2)	C_{dl} (F/cm^2)
P-zeolite nanocomposite	1 day	3.64×10^2	2.350×10^3	7.435×10^{-6}
	7 days	2.98×10^2	1.735×10^3	2.014×10^{-5}
	14 days	1.02×10^2	1.200×10^3	2.051×10^{-5}
	21 days	1.47×10^2	1.130×10^3	1.651×10^{-5}
	28 days	0.85×10^2	0.650×10^3	3.154×10^{-4}
Zn-P-zeolite nanocomposite	1 day	6.308×10^3	18.500×10^3	3.101×10^{-6}
	7 days	4.010×10^3	14.535×10^3	3.004×10^{-6}
	14 days	4.218×10^3	11.200×10^3	3.801×10^{-6}
	21 days	1.602×10^3	10.420×10^3	3.662×10^{-5}
	28 days	1.534×10^3	8.515×10^3	4.043×10^{-5}
Cu-P-zeolite nanocomposite	1 day	2.700×10^3	10.527×10^3	3.405×10^{-6}
	7 days	1.805×10^3	9.823×10^3	5.142×10^{-6}
	14 days	1.015×10^3	7.945×10^3	2.361×10^{-6}
	21 days	7.530×10^2	5.521×10^3	7.651×10^{-5}
	28 days	7.687×10^2	4.667×10^3	9.124×10^{-5}
(Zn/Cu)-P-zeolite nanocomposite	1 day	9.926×10^3	41.512×10^3	1.051×10^{-6}
	7 days	7.021×10^3	23.713×10^3	2.614×10^{-6}
	14 days	6.321×10^3	23.020×10^3	2.031×10^{-6}
	21 days	6.219×10^3	18.000×10^3	3.051×10^{-6}
	28 days	2.119×10^3	14.520×10^3	5.245×10^{-6}

The standard deviation for R_s is 4.2–12%

The standard deviation for R_{ct} is 2.5–8.9%

The standard deviation for C_{dl} is 2.3–10.8%

active release of antibacterial agents. Their small particle size promotes larger specific surface area, increasing the possibility of coming into contact with the bacterial cell membrane and facilitating penetration and damage.[28–30]

Generally, the results show that the (Zn/Cu)-P-zeolite offered the best anticorrosive and antibacterial actions due to the co-release of both Zn and Cu via different mechanisms simultaneously, exhibiting a dual effect compared with the single-release coatings, resulting in their enhanced anticorrosive and antibacterial behavior. These results are in good agreement with results in literature showing that modified zeolite offers the highest corrosion resistance for bare metal in saline solution, being superior to epoxy ester coating formulations.[8]

Based on EIS data as well as SEM/EDX surface analysis, inclusion of Na*X* zeolite particles doped with

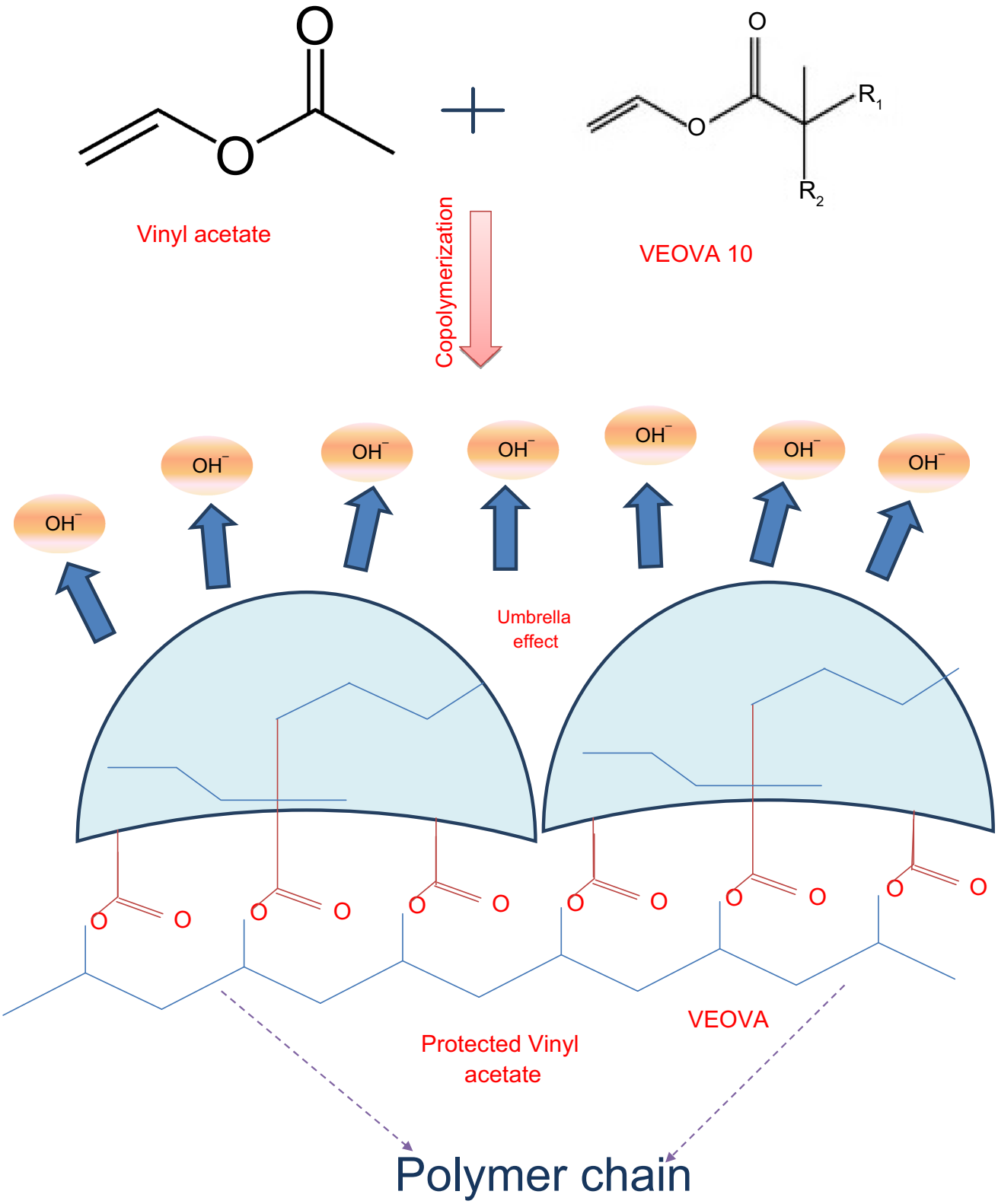

Fig. 8: Schematic of the umbrella effect of VEOVA 10

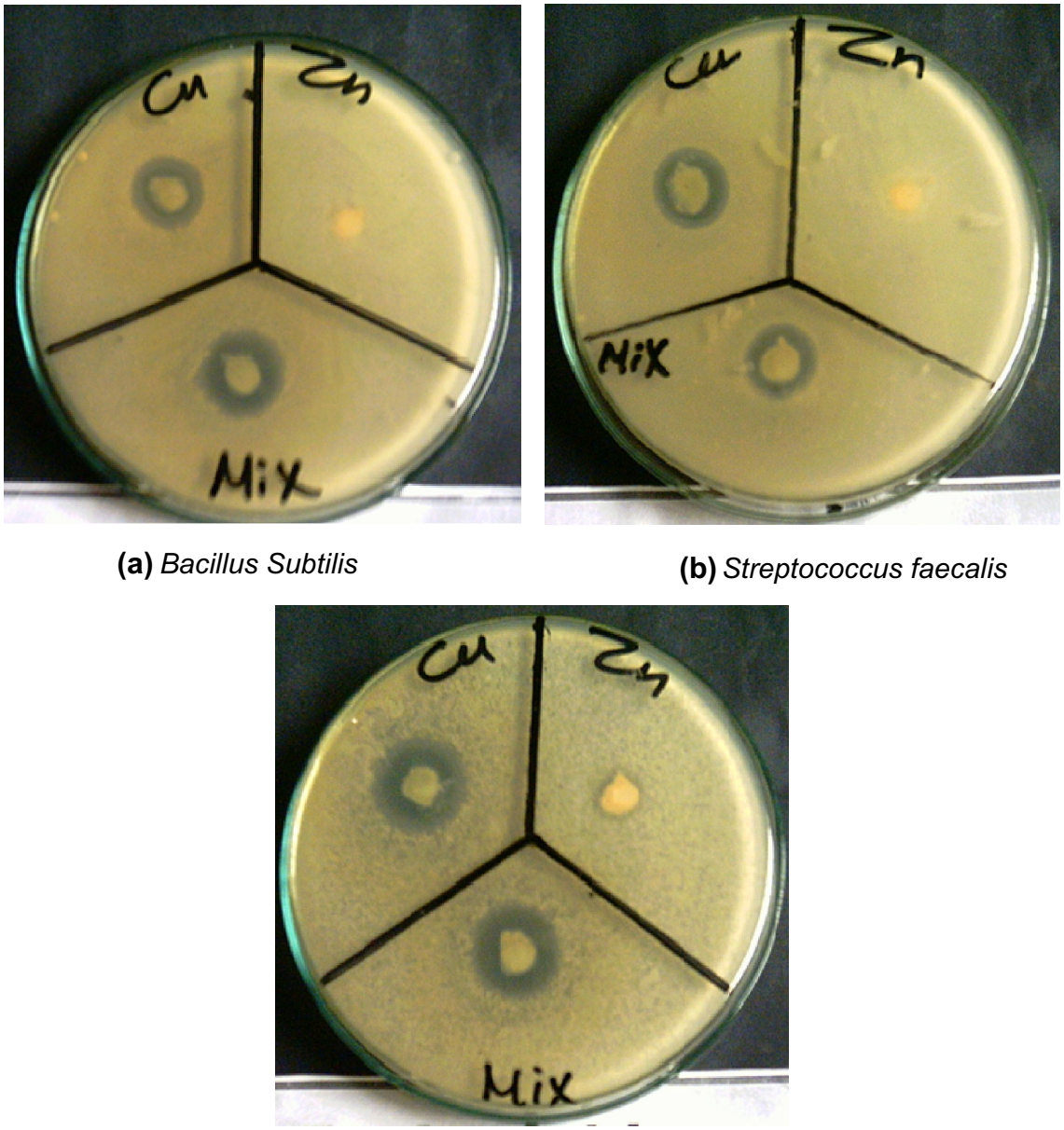

(a) *Bacillus Subtilis*

(b) *Streptococcus faecalis*

(c) *Escherichia coli*

Fig. 9: Inhibition zone of cation-exchanged P-zeolites

Zn^{2+}/2-mercaptobenzimidazole (MBI) in epoxy ester film led to active corrosion protection, prolonging the coating lifetime, which shows a synergistic effect.[8] Also, according to Bakhsheshi-Rad et al.,[10] silver-zeolite-doped hydroxyapatite coating (Ag-Zeo-HAp) offered good bioactivity, high antibacterial performance, and high corrosion protection for TiO_2-coated

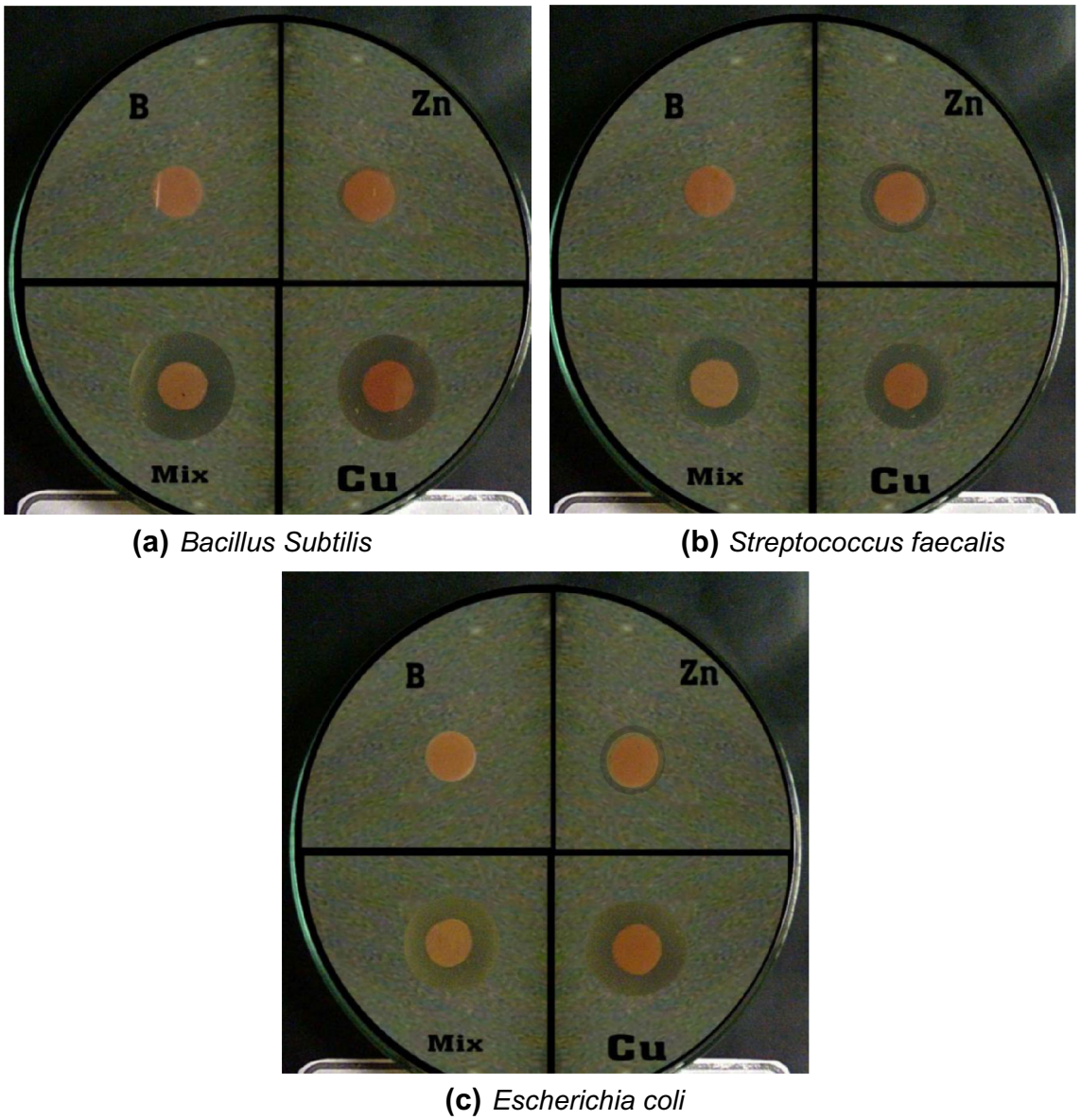

(a) *Bacillus Subtilis* **(b)** *Streptococcus faecalis*

(c) *Escherichia coli*

Fig. 10: Inhibition zone of the four prepared nanocomposites containing zeolites

Mg alloy, but it is well known that silver is very expensive.

Based on the results described above and their comparison with results in literature, it can be concluded that cation-exchanged P-zeolites could be applied successfully in both anticorrosive and antibacterial coatings, enabling cost-saving multifunctional coatings with long-term durability and easy preparation using a simple cation-exchange process to replace the sodium cation with other appropriate cations for use in different fields. Such coatings will help decrease corrosion and bacterial infection by keeping critical locations safer, cleaner, and less infectious.

Table 8: Antibacterial activity of cation-exchanged P-zeolites and the painted specimens

Powder Sample	Inhibition zone diameter (mm per 1-cm sample)		
	Bacterial species		
	G^+		G^-
	Bacillus subtilis	*Streptococcus faecalis*	*Escherichia coli*
Antibacterial activity of cation-exchanged P-zeolites			
Zn-P-zeolite	0	0	10 ± 0.5
Cu-P-zeolite	17 ± 0.5	17 ± 0.5	19 ± 0.5
(Zn/Cu)-P-zeolite	21 ± 0.5	18 ± 0.1	19 ± 0.5
Antibacterial activity of paints			
Blank (B)	0	0	0
In situ Zn-P-zeolite-copolymer nanocomposite	13R ± 0.5	16 ± 0.1	13 ± 0.1
In situ Cu-P-zeolite copolymer nanocomposite	30 ± 0.4	25 ± 0.5	27 ± 0.5
In situ (Zn/Cu)-P-zeolite-copolymer nanocomposite	32 ± 0.5	26 ± 0.1	27 ± 0.5

Most samples showed antibacterial activity against the tested microorganisms

Inhibition zone expressed as mean ± standard deviation (mm)

R Repellent action (not complete inhibition), *G* Gram reaction

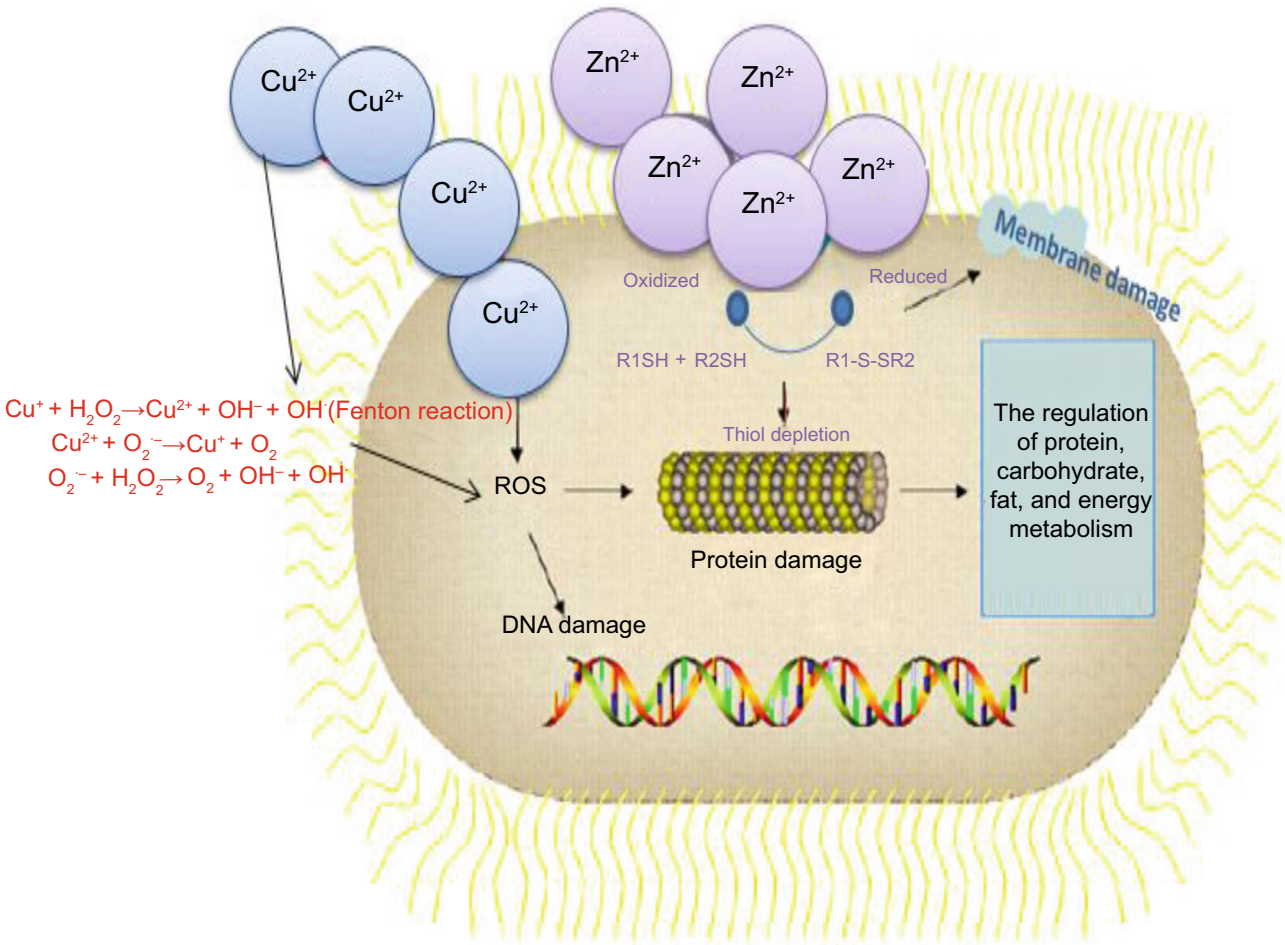

Fig. 11: Schematic of antibacterial mechanisms

Conclusions

P-zeolite was prepared from a cheap ore (Egyptian kaolin) and subjected to a cation-exchange process to replace Na^+ by Zn^{2+}, Cu^{2+}, or their mixture. Based on the results, the following conclusions can be drawn:

1. P-zeolite and the cation-exchanged P-zeolites were mixed with vinyl acetate-vinyl versatate (VAc-VEOVA) copolymer at the nanoscale via an in situ polymerization process to form four nanocomposites, namely P-zeolite-(VAc-VEOVA), Zn-P-zeolite-(VAc-VEOVA), Cu-P-zeolite-(VAc-VEOVA), and Zn/Cu-P-zeolite-(VAc-VEOVA).
2. The anticorrosion performance of paints containing the four nanocomposites was estimated using immersion testing and EIS measurements, revealing corrosion protection performance in the order: (Zn/Cu)-P-zeolite > Zn-P-zeolite > Cu-P-zeolite > P-zeolite.
3. Antibacterial activity testing of the paint films revealed the best performance for the (Zn/Cu)-P-zeolite-(VAc-VEOVA) nanocomposite.
4. Overall, the (Zn/Cu)-P-zeolite exhibited the best performance in terms of both anticorrosion and antibacterial behavior.

References

1. Montemor, MF, ''Functional and Smart Coatings for Corrosion Protection: a Review of Recent Advances.'' *Surf. Coat. Technol.*, **258** 17–37 (2014)
2. Zvonkina, IJ, Hilt, M, ''Strategies for Developing Multifunctional, Self-Healing Coatings for Corrosion Prevention and Other Functions''. In: Makhlouf, ASH (ed.) *Handbook of Smart Coatings for Materials Protection*. 105–120 (2014) Woodhead
3. Wang, C, Wang, H, Hu, Y, Liu, Z, Lv, C, Zhu, Y, Bao, N, ''Anti-corrosive and Scale Inhibiting Polymer-Based Functional Coating with Internal and External Regulation of TiO_2 Whiskers.'' *Coatings*, **8** (2018). https://doi.org/10.3390/coatings8010029
4. Victor, A, David, V, Zegui, Y, Lan, N, Ore, K, ''*High Quality Vinyl Ester Based Binders for Elastomeric Roof Coatings*.'' www.abrafati2017.com.br/2013/Dados/PDF/Paper_118.pdf. Accessed 2013
5. Vanaken, D, Arriaga, V, ''Branched Vinyl Ester Monomers for Hydrophobic Emulsion Polymers.'' *Proceedings of the 40th Annual International Waterborne, High Solids, and Powder Coatings Symposium*, 117–131 (2013)
6. Deya´, C, Romagnoli, R, delAmo, B, ''A New Pigment for Smart Anticorrosive Coatings.'' *J. Coat. Technol. Res.* **4** 167–175 (2007)
7. Ferrer, EL, Rollon, RP, Lafont, U, Mendoza, HD, García, SJ, ''Double-Doped Zeolites for Corrosion Protection of Aluminium Alloys.'' *Microporous Mesoporous Mater.*, **188** 8–15 (2014)
8. Rassouli, L, Naderi, R, Mahdavain, M, ''Study of the Active Corrosion Protection Properties of Epoxy Ester Coating with Zeolite Nanoparticles Doped with Organic and Inorganic Inhibitors.'' *J. Taiwan Inst. Chem. Eng.*, **85** 207–220 (2018)
9. Calabrese, L, Bonaccorsi, L, Capr, A, Proverbio, E, ''Effect of Silane Matrix on Corrosion Protection of Zeolite Based Composite Coatings.'' *La Metallurgia Italiana*, **106** 35–39 (2014)
10. Bakhsheshi-Rad, R, Hamzah, E, Ismail, AF, Aziz, M, Karamian, E, Iqbal, N, ''Bioactivity, In Vitro Corrosion Behavior, and Antibacterial Activity of Silver-Zeolites Doped Hydroxyapatite Coating on Magnesium Alloy.'' *Trans. Nonferrous Met. Soc. China*, **28** 1553–1562 (2018)
11. Salim, MM, Malek, NANN, ''Characterization and Antibacterial Activity of Silver Exchanged Regenerated NaY Zeolite from Surfactant-Modified NaY Zeolite.'' *Mater. Sci. Eng. C*, **59** 70–77 (2016)
12. Yeh, J, Chang, K, ''Review, Polymer/Layered Silicate Nanocomposite Anticorrosive Coatings.'' *J. Ind. Eng. Chem.*, **14** 275–291 (2008)
13. Suarez-Martinez, PC, Robinson, J, An, H, Nahas, RC, Cinoman, D, Lutkenhaus, JL, ''Polymer-Clay Nanocomposite Coatings as Efficient, Environment Friendly Surface Pretreatments for Aluminum Alloy 2024-T3.'' *Electrochim. Acta*, **260** 73–81 (2018)
14. Olad, A, Naseri, B, ''Preparation, Characterization and Anticorrosive Properties of a Novel Polyaniline/Clinoptilolite Nanocomposite.'' *Prog. Org. Coat.*, **67** 233–238(2010)
15. Nasr, HE, Mohamed, WS, ''In Situ Emulsion Polymerization of Terpolymer/Montmorillonite Nanocomposites Using Redox Initiation System.'' *J. Am. Sci.*, **6** 1195–1201 (2010)
16. Kongparakul, S, Kornprasert, S, Suriya, P, Le, D, Samart, C, Chantarasiri, N, Prasassarakich, P, Guan, G, ''Self-Healing Hybrid Nanocomposite Anticorrosive Coating from Epoxy/Modified Nanosilica/Perfluorooctyltriethoxysilane.'' *Prog. Org. Coat.*, **104** 173–179 (2017)
17. Sabbah, IA, Mohamed, TA, Nasr, HE, Emam, SE, *Int. J. Collabor. Ent.* 5 (2015)
18. Unzue, MJ, Asua, JM, *J. Appl. Polym. Sci.* **49** (1993)
19. Huo, Z, Xu, X, Lv, Z, Song, J, He, M, Li, Z, ''Thermal Study of NaP Zeolite with Different Morphologies.'' *J. Therm. Anal. Calorim.*, **22** 1–5 (2012)
20. Zubowa, HL, Kosslick, H, Muller, D, Richter, M, Wilde, L, Fricke, R, ''Crystallization of Phase-Pure Zeolite NaP from MCM-22-Type Gel Compositions under Microwave Radiation.'' *Microporous Mesoporous Mater.*, **109** 542–548 (2008)
21. Rassouli, L, Naderi, R, Mahdavain, M, ''The Role of Micro/Nano Zeolites Doped with Zinc Cations in the Active Protection of Epoxy Ester Coating.'' *Appl. Surf. Sci.*, **423** 571–583 (2017)
22. Dias, SAS, Lamaka, SV, Nogueira, CA, Diamantino, TC, Ferreira, MGS, ''Sol-Gel Coatings Modified with Zeolite Fillers for Active Corrosion Protection of AA2024.'' *Corr. Sci.*, **62** 153–162 (2012)
23. Ahmed, NM, Abd El-Gawad, WM, El_Shami, AA, Souaya, EMR, ''Electrochemical Studies on the Corrosion Performance of New Advanced Anticorrosive Pigments.'' *Pigm. Resin Technol.* **46** 181–193(2017)
24. Lemire, J, Harrison, JJ, Turner, RJ, ''Antimicrobial Activity of Metals: Mechanisms, Molecular Targets and Applications.'' *Nat. Rev. Microbiol.*, **11** 371–384 (2013)
25. Workentine, ML, Harrison, JJ, Stenroos, PU, Ceri, H, Turner, RJ, ''*Pseudomonas fluorescens*' View of the Periodic Table.'' *Environ. Microbiol.*, **10** 238–250 (2008)
26. Nies, DH, ''Efflux-Mediated Heavy Metal Resistance in Prokaryotes.'' *FEMS Microbiol. Rev.*, **27** 313–339 (2003)
27. Harrison, JJ, Ceri, H, Turner, RJ, ''Multimetal Resistance and Tolerance in Microbial Biofilms.'' *Nat. Rev. Microbiol.*, **5** 928–938 (2007)

28. Cloutier, M, Mantovani, D, Rosei, F, ''Review Antibacterial Coatings: Challenges, Perspectives, and Opportunities.'' *Trends Biotech.*, **33** 637–652 (2015)
29. Hadidi, M, Bigham, A, Saebnoori, E, Hassanzadeh-Tabrizi, SA, Rahmati, S, Alizadeh, ZM, Nasirian, V, Rafienia, M, ''Electrophoretic-Deposited Hydroxyapatite-Copper Nanocomposite as an Antibacterial Coating for Biomedical Applications.'' *Surf. Coat. Technol.*, **321** 171–179 (2017)
30. Wang, L, Hu, C, Shao, L, ''The Antimicrobial Activity of Nanoparticles: Present Situation and Prospects for the Future.'' *Int. J. Nanomed.*, **12** 1227–1249 (2017)